Tellus (2006), 58A, 331–343
Printed in Singapore. All rights reserved

TELLUS

Radar-based precipitation type analysis in the Baltic area

By ANDI WALTHER[1]* and RALF BENNARTZ[1,2], [1]*Institut für Weltraumwissenschaften, Freie Universität Berlin, 12165 Berlin, Germany;* [2]*Department of Atmospheric and Oceanic Sciences, University of Wisconsin, Madison, Wisconsin, 53706, USA*

(Manuscript received 9 August 2005; in final form 19 December 2005)

ABSTRACT

A method to classify precipitation events based on their spatial extent and texture has been developed and applied to 3 yr of BALTEX Radar Data Center weather radar composites over the Baltic region. The method is capable of distinguishing large-scale precipitation features typically associated with frontal systems from more small-scale features, which are usually found in convective systems. Data used for this study are 2-D radar images. The classification is performed in three steps. First, contiguous precipitation areas are identified in the radar data. In the second step, each of these areas is subjected to an analysis where different texture parameters are calculated. In a third step, these texture parameters are evaluated by means of a neural network, and a type of precipitation is assigned to each class. The neural network has been trained using a large set of visually classified radar scenes. A validation of the results has been performed by (1) comparing regions where U.K. Met Office analysis shows large contiguous frontal areas and (2) by using surface observations where the surface observer reported precipitation events that could clearly be associated either with intermittent convective precipitation or with frontal systems. The results of the different comparisons are generally in good agreement with each other, and the false classification rate ranges from 10% to 20%.

The application to 3 yr of radar data has resulted in estimation of the frontal fraction of precipitation in the Baltic Sea area. About two-thirds of overall precipitation events are determined by frontal passages with high seasonal and diurnal variations.

1. Introduction

Currently the system earth–atmosphere appears to be in a phase of rapid global climate change. This change is reflected not only in an increase of globally averaged temperatures over the last century, but also in a change in the frequency of severe weather events and intensive storm systems in the mid-latitudes of the northern hemisphere. Global and regional climate models predict that these changes will be amplified in the future with possibly severe impacts on the earth's ecosystems as well as on human society. Possibly more important than changes in temperature will be changes in storm frequency and in the spatial and temporal distribution of precipitation. It is thus of interest to investigate precipitation in all aspects. There have been, however, only few studies on the relationship of rain amount and synoptic situation in the mid-latitudes.

The Global Energy and Water Cycle Experiment (GEWEX) has been organized by the World Meteorological Organization (WMO) to foster the understanding of the global hydrological cycle. As part of GEWEX, regional subexperiments have been established to study the water balance over major catchment areas. The Baltic Sea Experiment (BALTEX) is the European subexperiment of GEWEX with emphasis on the Baltic Sea. The BALTEX main observational period (BRIDGE) took place between 1999 April and 2001 March. Within BALTEX-BRIDGE, the Swedish Meteorological and Hydrological Institute (SMHI) established the BALTEX Radar Data Center (BRDC, Michelson et al., 2000).

The Baltic Sea is a semi-enclosed sea. Its climate is strongly affected by prevailing cyclones activities. The annual estimate of precipitation is about 700 mm with a maximum in August (about 80 mm/month) and minimum in April (40 mm/month) (Skomorowski et al., 2003). The water body of the Baltic Sea covers about 415 000 km^2, while its catchment area is about four times as large. The radar data composites used in this study cover 95% of the Baltic Sea and about 75% of the catchment. The questions we wish to address using this data set are:

(i) What is the fraction of precipitation events directly associated with frontal overpasses?

*Corresponding author.
e-mail: andi.walther@wew.fu-berlin.de
DOI: 10.1111/j.1600-0870.2006.00183.x

(ii) What is the diurnal, annual and interannual variability of this fraction?

Previous radar work has mainly emphasized the distinction between different types of cloud microphysical processes that trigger precipitation. These classifications typically assign a precipitation event either the classes stratiform or convective based on the main cloud microphysical processes that drive the precipitation event (e.g. Steiner et al., 1995; Biggerstaff and Listemaa, 2000; Anagnostou and Kummerow, 1997). While these classifications are of great importance to understand the day to day variability of radar observations and the variability in the relation between rain rate and radar reflectivity, they clearly cannot serve to answer the above questions. This is even more the case since we are concerned with precipitation on scales of several hundred to thousand kilometres, which cannot be fully three-dimensionally covered by a single ground based weather radar.

Rainfall characteristics are strongly linked to the synoptic weather situation in which the events occur. Sumner (1988) defined three main types of precipitation in terms of the initial processes as follows: orographic, frontal and convective. Shepherd et al. (1988) suggested the application of space–time correlation analysis to radar data in order to divide into showery and frontal precipitation. Tetzlaff and Hagemann (1986) analysed the precipitation type by means of synoptical weather observations of the Hannover-Herrenhausen station (North Germany) for a period of 6 yr (1979–1984). The rain events were subdivided into several classes according to the synoptic situation that triggered the precipitation event. About 60% of the total precipitation fell in association with frontal systems. The classification approach builds on this work and is thus not strictly microphysical but distinguishes between different types of precipitation based on the large-scale characteristics of radar composites. Such characteristics include the horizontal extent of individual precipitating systems, their spatial homogeneity, as well as their temporal variation. We show that this classification is able to distinguish between precipitation events associated with fronts and precipitation events that are triggered by isolated convective processes. Both the terms 'frontal' and 'convective' are hereafter used to describe the weather situation that triggers the precipitation event and not the microphysical processes that lead to precipitation formation. Obviously, it is possible for precipitation within a front to form via strong updrafts, thus being convective in a microphysical sense (embedded convection). Similarly, even the most intensive convectively driven precipitation events usually consist of parts where precipitation generation is driven by stratiform processes (e.g. stratiform tail). It is, therefore, important to note that we use the terms frontal and convective in a synoptic sense and not in a microphysical sense.

Our classification approach is subjective in nature and depends on the human observer in a similar way as, for example, satellite cloud classifications depend on the human observer. An automatic classification based on the training by a human observer can hardly ever supersede the individual human classification. However, automated approaches allow the classification of large data sets in a fast and efficient manner. In fact, the same human observer might classify different cloud or precipitation systems differently when they are presented to him twice. An automatic classification approach will—after training—yield consistent results based on a subjective, but stable, set of decision rules.

Artificial neural networks (ANNs) have been employed in a number of studies for the classification of clouds using textural features as input parameters (Pankiewicz, 1997; Tian et al., 1999). These studies indicate that the use of neural network is well suitable for classifying typical patterns in remote sensed images.

This article is organized as follows: The radar data set is described in Section 2. The development and architecture of the method is explained in Section 3. To improve legibility, the technical details of the method are summarized in Appendix A. We undertake some effort to derive the uncertainty range associated with the classification and to show that its accuracy does not depend on, for example, seasonal variations in precipitation. These results are summarized in Section 4. Section 5 shows the results of the application to 3 yr of BALTRAD data. Finally, Section 6 summarizes the main findings of this study.

2. The BALTRAD data set

The data used for this study are composite images from the BALTRAD radar network compiled at the BRDC. The BRDC has been established at the Swedish Weather Service (SMHI) for collecting data from as many precipitation radars in or adjacent to the Baltic Sea catchment area as possible, deriving homogenous data sets, distributing them to BALTEX data users, and archiving the data sets. The products are presented in detail in Michelson et al. (2000). Most of these radars operate in the C-Band (5 cm wavelength), while two radars operate in the X-band (3 cm). BALTRAD data products include radar reflectivity images of each of the 30 radar stations, composite images of radar reflectivity factor and images for three and twelve hour precipitation sums. Additionally, gauge-adjustment factors derived using collocated rain gauge measurements are produced.

The weather radar composite images used in this study contain 815 $\times$ 1195 pixel. Each pixel represents a 2 $\times$ 2 km area within an equal area Lambert projection. The temporal resolution is 15 min. For the purpose of this study and in accordance with Michelson et al. (2000), instantaneous composite images of the radar reflectivity factor Z (in dBZ) were converted to 2-D precipitation images containing rain rate R (in mm hr^{-1}) using a standard Marshall-Palmer relation $Z = aR^b$ with $a = 400$, $b = 2$ for the cold season (October to March) and $a = 200$, $b = 1.6$ for the warm season (April to September). Systematic range-dependent biases are removed using the gauge adjustment factor as described in Michelson et al. (2000). Afterwards the

rain rates of each scene were re-transformed into corresponding quasi-reflectivity factors for further examination. Three years of data—from 2000 January to 2002 December—were used for the development and application of the methodology. Two isolated radars (over Poland) had to be excluded from the investigation because the missing overlap with the other radar prevented any spatial analysis on data taken from those radars.

When using ground based radar data, serious complications arise, especially using quantitative rain rates. The high sensitivity of rain intensity to errors in radar reflectivity factor result in a high uncertainty in any instantaneous rain rate. Further, despite several carefully applied correction algorithms for ground clutter, beam blocking, and anomalous propagation (Michelson et al., 2000), inhomogeneities and errors in accumulated precipitation maps generated from this data set—as well as from any other data set based on ground based weather radar—can also not be completely avoided. Those uncertainties have to be accounted for in uncertainty estimates that go along with the described method.

3. Methodology

We first describe the general algorithm flow before we discuss the single steps in detail. Figure 1 shows a top level diagram of the classification approach. Generally speaking, we use the texture information of the corrected radar reflectivity factor of precipitation systems in combination with an ANN in order to distinguish frontal and convective precipitation. Pankiewicz (1997) suggested a similar technique for classifying shallow and deep convective air masses from satellite data as an estimate of convective precipitation. In that study the textural parameters within clippings of a fixed size were used as input parameters of a neural network algorithm. In contrast to that approach textural and geometrical parameters of of entire contiguous precipitation systems have been used here.

Based on an individual radar composite image, we first identify contiguous precipitation areas. If these areas are smaller than a predefined size of 4000 km^2 they are initially assigned 'convective'. If the individual precipitation events are larger than this threshold several texture parameters are derived for each of these precipitation areas. These parameters are then used as input for an ANN that decides on whether each individual case is convective or frontal. In the next step all precipitation events within 20 km distance from a frontal precipitation event are assigned as frontal. In a similar manner the temporal neighbourhood of a frontal system is assigned frontal for all images within 60 min around the current image. Subsequently, we describe the different steps in detail and illustrate the approach based on sample images.

3.1. Identification of contiguous rain areas

Contiguous rainfall areas are determined using an algorithm with an eight-connected neighbourhood definition, that is, the algorithm searches for neighbouring pixels with rain rate or radar reflectivity (or, more generally, grey value) greater than a certain threshold not only in horizontal, but also in diagonal directions. The examination technique is based on a region growing technique similar to that described in Schowengerdt (1997). Each connected rainfall area is labelled with a unique region index. Included non-precipitation pixels do not count as a part of the labelled area. For our purposes we use a threshold of 2 dBZ (corresponds to about 0.05 mm hr^{-1} for warm season and about 0.07 mm hr^{-1} in cold season) to delineate different areas. The result of this process is an image with N identified contiguous areas of precipitation larger than 4000 km^2. The threshold of

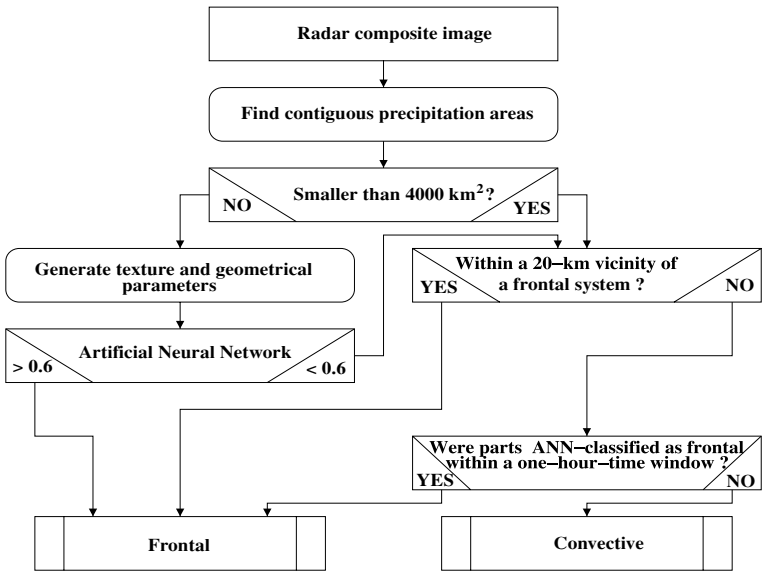

Fig. 1. Flow diagram of the classification algorithm.

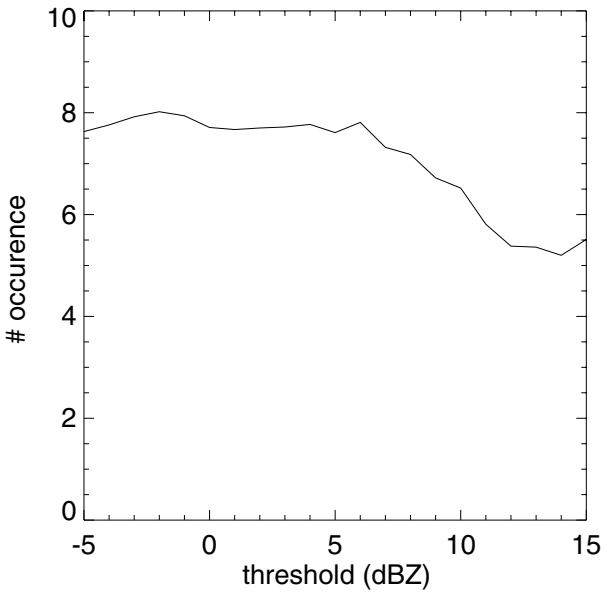

Fig. 2. Average number of contiguous precipitation fields in a single image as a function of wet pixel threshold.

2 dBZ has been found empirically by trying to obtain as stable results as possible with respect to the number of identified precipitation events per image. This is shown in Fig. 2, where the average number of precipitation events found in one image as a function of the threshold value is plotted for several hundred randomly chosen images. It can be seen that the number of large precipitation areas is almost constant in a range between −5 dBZ and 8 dBZ. We conclude that the classification results are insensitive to the particular choice of the threshold as long as it is not extremely low (smaller than −5 dBZ) or extremely high (larger than about 8 dBZ). Besides small modifications in size and shape, the choice of the threshold in the above-mentioned range leads mostly to almost identical precipitation areas.

The size of the contiguous areas is then used to preliminarily assign a class to each of the precipitation events as shown in Fig. 1. That means that small areas (less than 4000 km^2) are preliminarily assigned convective, whereas large areas are further processed as described below.

3.2. Parameters to describe a precipitation system

For precipitating areas larger than the aforementioned size, it is initially unclear whether they are associated with a frontal system or not. The human observer can visually classify those events, but also with a non-negligible false alarm rate as discussed below. The human observer relies on texture and shape features to identify precipitation and our classification resembles this particular capability. A large horizontal extent as well as the elongated shape and smooth variations of rain rate or radar reflectivity can be identified with frontal rain bands. In contrast, intermittent and spatially highly variable rain events are identified as convective precipitation. We prescribe eight values for each precipitation area that has been identified within the image to capture these features. These four texture parameters and four shape descriptors are introduced in the appendix. They form an input vector that is subsequently used to characterize precipitation events by type.

3.3. Development of the classification tool

A supervised back-propagation ANN is used as a classification tool. Back-propagation ANNs are able to "learn" the functional relation between a set of i input vectors $\mathbf{x}_i$ and output vectors $\mathbf{y}_i$. A training data set $[\mathbf{x}_i, \mathbf{y}_i]$ has to be provided to the ANN to learn the relation between $\mathbf{x}_i$ and $\mathbf{y}_i$ before it can be used to independently classify new sets of $\mathbf{x}_i$. A first test on the performance of the ANN is usually obtained by creating a second independent set of $[\mathbf{x}_i, \mathbf{y}_i]$ called a test data set. It allows one to quantify how well the ANN is able to generalize the learned relation.

3.3.1. Selection of the training data set. The first step in training a neural net is to find a data set $[\mathbf{x}_i, \mathbf{y}_i]$ that can be used for training. This data set has to be sufficiently large to span the full range of expected variability of the input vector $\mathbf{x}_i$. For our particular case, we used an approach to randomly select weather radar images from 2001 to 2002 and within each scene we again randomly picked several precipitation events that were then classified visually. The re-analyse maps of UKMO (example in Fig. 3) gave additional indications of the actual synoptical situation. Each of these events was then stored as a vector $[\mathbf{x}_i, \mathbf{y}_i]$, where $\mathbf{x}_i$ are the aforementioned eight structural parameters and $\mathbf{y}_i$ is either zero if the event was visually classified as convective or one if it was classified as frontal. After several thousands of these visual classifications the data set was homogenized so that frontal and convective cases occur with roughly the same likelihood. Finally, it was split into two data sets, one for training and one for testing.

3.3.2. Statistical properties of the training data set. Before we proceed with the neural network training, it is worthwhile to study the statistical properties of the training data set. This will allow us to draw some first conclusion on how well the various texture and geometrical parameters are correlated with the visual classification of the training data set. It is also possible to find high cross-correlations among some of the input features to potentially reduce the dimensionality of the input data set to prevent the neural network from being trained with redundant input variables.

Table 1 shows the cross-correlation analysis for the set of training data $[\mathbf{x}_i, \mathbf{y}_i]$. The last row gives the correlation between the various input parameters and the visual classification. A positive classification here indicates that if the respective parameter has a high value, the event is more likely to be frontal.

The mean grey value difference (GVD) is weakly negatively correlated with the visual classification which indicates that if

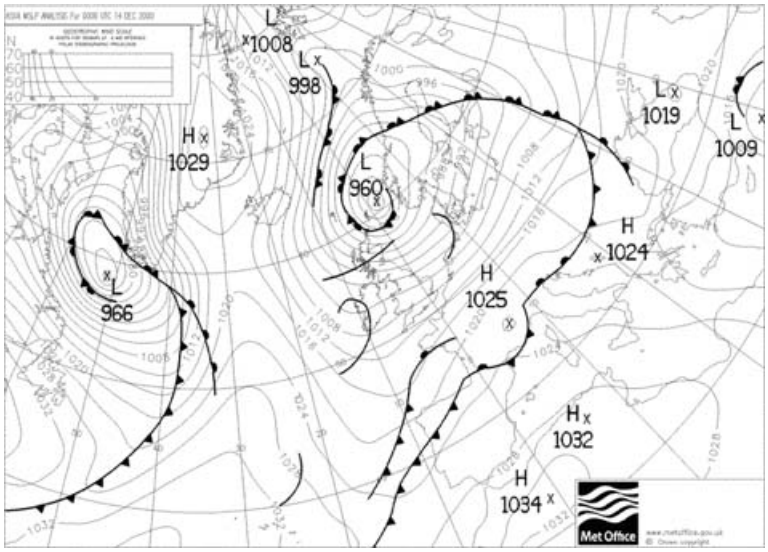

Fig. 3. Re-analyse map of 00 UTC 14 December 2000 by courtesy of U.K. Metoffice ((c) British Crown copyright 2005, Published by the Met Office).

the mean differences between the adjacent pixels in the feature are getting smaller, it is more likely to be frontal. The highest positive correlation is found for the size of the major axis and the relative amount of raining pixels in the box around the feature as defined by the minor and major axis. Both show a correlation of about 0.8, which indicates that larger precipitation events are more likely to be associated with fronts and that events which are more regularly filled with precipitation are more likely to be frontal.

Looking at the cross-correlations between the different input parameters one finds maximum absolute correlations slightly smaller than 0.9 between entropy and mean difference as well as between the overall size of the area and its major axis. These parameters are obviously correlated since an increase in the mean difference corresponds to an increase in the average disorder, and hence entropy, of the system. Interestingly, even though both features are correlated to some extent their correlation with the classification is very different.

We use a multilayer perceptron neural network (Marquard, 1963; Rumelhart and McClelland, 1986) with an input layer of eight neurons for the eight texture and shape parameters, a hidden layer of 25 neurons and one output neuron that varies between zero (convective) and one (frontal). The transfer function at each node is sigmoidal.

Figure 4 shows the number of classified precipitation events as a function of their horizontal extent in km^2. Small precipitation events (less than 15 000 km^2) are almost exclusively classified as convective. Between 15 000 km^2 and 50 000 km^2 the classification is not unique and the precipitation event might be either convective or frontal depending on its shape and texture. Very large features (larger than 60 000 km^2) are entirely classified as frontal. For sizes around 30 000 km^2 about 50% of the precipitation events are classified frontal and about 50% convective. Note that even though most of the individual precipitation events are small, the contribution of a precipitation event to the total rainfall is to first order proportional to its horizontal extent, so that the medium-sized precipitation events contribute significantly to the total rain rate.

The upper third of Table 2 states the results of the classification of the test data set. The false alarm rate lies at six percent.

Table 1. Cross-correlation matrix of the input and output parameters of the neural network

	1	2	3	4	5	6	7	8	9
1 mean	1								
2 homogeneity	−0.68	1							
3 entropy	0.86	−0.76	1						
4 contrast	0.81	−0.50	0.47	1					
5 size	−0.36	0.24	−0.23	−0.39	1				
6 major axis	−0.37	0.20	−0.20	−0.43	0.89	1			
7 eccentricity	0.07	0.08	0.00	0.09	−0.06	−0.25	1		
8 compactness	−0.63	0.41	−0.44	−0.67	0.72	0.76	−0.02	1	
9 frontindex	−0.39	0.25	0.78	−0.45	0.69	0.80	−0.16	0.78	1

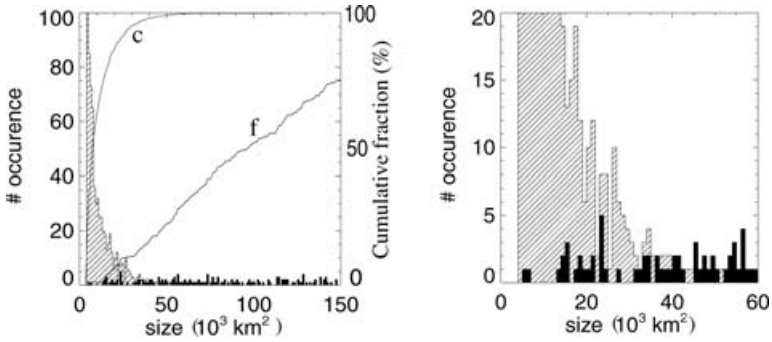

Fig. 4. Frequency of occurrence of precipitation areas of specific type as a function of size. The left image shows the result of the entire range of size (Filled: frontal, streaked: convective). Solid lines indicate the cumulative function of frontal (f) and convective (c) events. The right image displays the clipping of the size range smaller than 60 000 km^2.

Table 2. Parameters and skill of the test data set, the validation with UKMO analysis fields and the validation with SYNOP. (N: number of trials, F: fraction of frontal events, V: Hanssen and Kuipers discriminant, HIT$_f$: hit rate of frontal events, HIT$_c$: hit rate of convective events, HIT: overall hit rate, FAD: false alarm detection.)

	Type of data	N	F	V	HIT$_f$	HIT$_c$	HIT	FAD
Test data	regions	445	23%	0.80	0.84	0.96	0.94	0.06
UKMO	pixels	$6.12 \cdot 10^6$	63%	0.81	0.89	0.92	0.91	0.09
SYNOP	observations	13856	65%	0.54	0.81	0.73	0.78	0.22

3.3.3. Temporal and spatial adjustments. After the neural network classification has been completed, two more steps are performed before the final classification is produced. In the first step, isolated precipitation events close to a frontal precipitation event are classified as a part of the latter frontal area. The search radius used for this adjustment is 20 km and hence very small given the typical extent of a frontal system. In the case study displayed in Fig. 5, some small isolated features can be identified at the north eastern part of the frontal system (64°N/30°E) that just by their size would have been identified as convection. It is clear, however, that they belong to the front. Similarly, at the south western part (64°N/15°E) a somewhat larger patch has been identified as frontal. Further south, two more patches can be identified which are not within the search radius and, therefore, remain convective. It is unclear whether these precipitation events belong to the front and this question could also not be answered by using auxiliary data such as the weather map or Meteosat infrared image.

Obviously, fronts that enter the observation area might initially be misclassified as convection just because only a small fraction of the entire frontal area can be seen by the radars. We, therefore, add a second temporal criterion to minimize this particular error source. For every event that has been classified as convective, we search earlier and later images if a frontal event has been detected in the same geographical region. If so, the event is classified as frontal, too. The search window is one hour.

Subsequently we describe a case study that highlights some of the uncertainties associated with the classification method. From looking at this example, it is clear that a 100% accuracy cannot be achieved and the definition of frontal and convective is fuzzy to some extent. A quantitative error analysis and evaluation of the classification is then provided in Section 4.

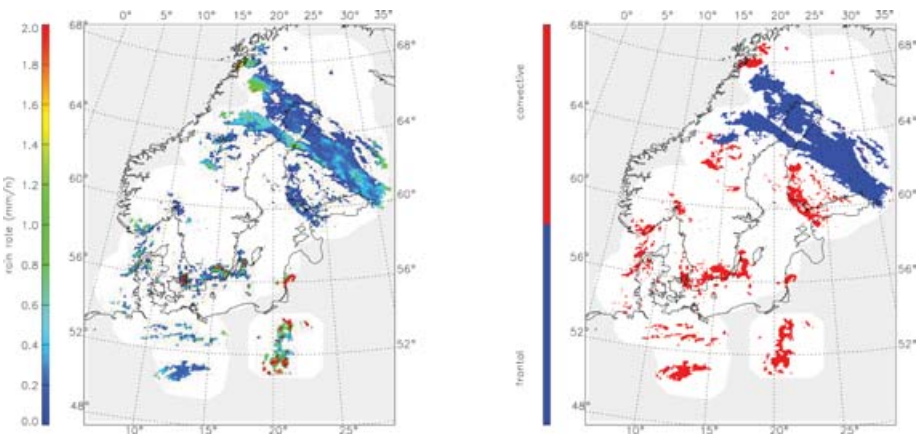

Fig. 5. Case study of 04:00 UTC 14 December 2000. The left image displays rain rate. The right image shows the frontal/non-frontal classification.

3.4. Case study

Figure 5 shows an example that utilizes the classification scheme. The image shows the radar reflectivities and the classification results for 04:00 UTC 2000 December 14. Figure 3 gives an overview over the synoptical situation in Europe. The Baltic area was influenced by a low-pressure system with its centre west of Norway. An occluded front covers the northern part of the bay of Bothnia. Isolated convective clouds can be identified over Poland, Denmark and northeastern Germany. The corresponding radar image shows the rain band over the bay of Bothnia, as well as isolated precipitation events associated with the post-frontal precipitation. The classification (right panel) correctly identifies the large-scale precipitation event as frontal and the small-scale events as convective. Some of the small-scale features close to the front are also assigned frontal due to the aforementioned spatial and temporal tests. However, several features close to the front appear to be not necessarily correctly identified. The small rain band over southern Finland is classified as convective, but an observer would intuitively associate it with the frontal rain band and classify it as frontal. In the very northern part of the frontal area, several smaller convective events are assigned frontal. However, the northernmost precipitation events are identified as convective. Even if the observer used weather maps as auxiliary information, it would not be possible to doubtlessly assign these areas as belonging to the frontal precipitation event.

4. Validation

While rainfall is one of the most important parameters in the atmospheric sciences, it is difficult to measure and no single rainfall estimate can be used as a calibration reference for any other one. On the one hand, the classification we discuss here is easier to validate than the absolute amount of rainfall, since the only point where the absolute rainfall amount impacts the classification is the delineation of the different features within an image. As described above, this delineation is only modestly sensitive to the absolute rainfall amount and hence absolute calibration uncertainties do not affect the classification very strongly. On the other hand, the method depends on a classification performed by a human observer which makes it more difficult to validate. A third issue arises from the lack of suitable validation data that would allow judgment of the type of precipitation event with a higher accuracy. The use of weather forecasts from numerical weather prediction (NWP) models might, in principle, enable identification of frontal areas, but it is unclear whether these fronts are predicted at the right location. Furthermore, a procedure to identify the location of the front in the NWP field would have to be established. Such a procedure, though, would have a similar intrinsic uncertainty as the classification we want to validate. However, NWP analysis fields, weather maps, and geostationary satellite imagery certainly help in several cases where the location of fronts can be identified. The second remaining radar-independent source of information about rainfall are surface observations (SYNOP), which might give some information about the type of precipitation. We, therefore, use a two-folded approach to assess the accuracy of our method by first comparing it to visually classified UKMO analysis fields. Secondly, we compare it to the SYNOP data, identifying events that are more likely to be associated with a front or convection from the SYNOP.

Validation of detection algorithms that can only have two possible results needs to be formulated into skill scores of 2×2 contingency tables. Here the four possible combinations of the table are (a) correct classification of frontal precipitation (i.e. frontal in both data sets), (b) misclassified frontal cases (frontal in 'truth' data set and convective in output of algorithm), (c) misclassified convective cases (convective in 'truth' data set and frontal output of algorithm) and (d) correct classification of convective precipitation (convective in both). Woodcok (1976) discussed several common skill scores for Yes/No decision tables, such as Heidke skill score (Heidke, 1926; Brier and Allen, 1952) or Appleman score (Appleman, 1960). Most of them depend strongly upon the distribution of the trial conditions. This discrepancy can surely not be eliminated totally, but ensuring that both possible results are equally weighted in all samples leads to compatible rankings.

The Hanssen and Kuipers discriminant V (Hanssen and Kuipers, 1965) equals the relevance of the hit rates—hit_1 and hit_2 ranging from 0 to 1—of both possible events without respect to potential inequalities of the sample:

$$V = \frac{ad - bc}{(a+b)(c+d)} = \frac{a}{(a+b)} + \frac{d}{(c+d)} - 1 = hit_1 + hit_2 - 1$$

where V ranges between perfect, but inverse score ($V = -1$), random score ($V = 0$) and perfect score ($V = 1$). The variance of V gives a measure for the statistical significance and was also discussed in Woodcok (1976):

$$\sigma_V = \frac{N - 4(a+b)(c+d)V}{4N(a+b)(c+d)}$$

with N being the total number of elements in the sample. Highly skewed sample distributions lead to high uncertainties in the score and have a corresponding high variance value.

4.1. Comparisons with visually classified UKMO analysis fields

In a first step, we compare the results of the method to classifications based on the UKMO analysis. Despite the aforementioned issues, this validation is not just a mere quality check, but it also allows us to establish an error estimate associated with the visual classification of the UKMO data as a reference. For this purpose, we randomly selected 20 radar images for each month of the year 2000 and classified the type of precipitation events based on UKMO analysis maps by eye. Table 2 summarizes the

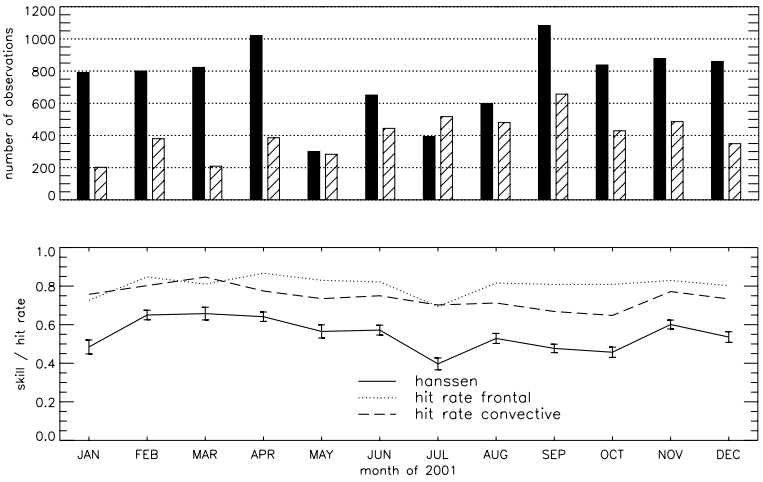

Fig. 6. Validation in dependency of month of 2001. (Top): Number of SYNOP observations (filled: frontal events, streaked: convective events. (bottom): hit rates and Hanssen and Kuipers skill parameter.

results of the comparison. In total, $6.12 \cdot 10^6$ single precipitation pixels were classified in both data sets, where 63% of the rain events were classified frontal and 37% convective by means of the UKMO maps. The classification method assigned 8.1% of the rain events convective, in cases where the observer assigned frontal. This is a relative false classification rate of about 13%. Similarly, 3.2% of the convective events are falsely classified as frontal, which corresponds to a relative false classification rate of about 10%. Therefore, a gross false classification rate of 10% can be assigned based on these results.

4.2. Comparisons with SYNOP

For the year 2001, we matched all available data from 390 synoptic stations with radar estimates for the same time and location. We then subdivided the SYNOP data into cases which were likely to be associated with frontal data, unclear cases, and cases which were likely to be associated with convection. The following criteria were used:

- A SYNOP observation was assumed to be frontal if the observer reported continuous rain or snow (weak, moderate, or heavy), no cumulonimbus and at least 5/8 cloud cover.
- A SYNOP observation was assumed to be convective if showers (rain, snow, graupel) were reported and cloud cover did not exceed 6/8.
- All SYNOP observations that did not fall into either category were rejected as unclassified.

Note that we are not interested in a classification of the SYNOP data itself. Rather we want to derive a subset of the SYNOP data and have a reasonable confidence that the selected cases are convective or frontal. Obviously, the above definition rejects several observations, and the data set was reduced to 9034 frontal and 4822 convective cases.

The results of the validation of the entire data set are summarized in the bottom row of Table 2. About 78% of the SYNOP observations were correctly classified, with a Hanssen and Kuipers score V of 0.54. The performance in detecting convective cases correctly was lower than that of frontal cases.

Fig. 6 shows seasonal variations in V. The upper panel illustrates the number of SYNOP observations. This number strongly depends upon the choice of criteria for the classification of the SYNOP data and does not represent any climatological 'truth', although the smaller likelihood of frontal precipitation in summer is well recognizable in the data.

V ranges between 0.4 and 0.65. A smaller number of convective observations leads to a higher V, which indicates a better performance in areas and times containing frontal precipitation.

Due to the spatial nature of the algorithm and the relatively large extent of the frontal areas, a number of incomplete frontal systems at the edge of the radar range might falsify the classification there. Fig. 7 shows the skill of the algorithm with respect to the distance to the edge of the radar range. It is seen that the variations in the skill score in respect to the distance to the edge are quite low.

5. Application to 3 yr of BALTRAD data

The method described in the previous sections has been applied to 3 yr of BALTRAD radar data (2000–2002). As a result we have obtained images of classification in which each pixel is grouped into either: (a) no measurement, (b) measurement, but no precipitation, (c) convective rain or (d) frontal rain. A statistical evaluation was conducted by analysing the frequency of precipitation events. Each pixel which hits or exceeds a given threshold of rain rate was counted as a precipitation event. The radar coverage was not stable over the entire period. The southern parts, mainly outside the Baltic Sea catchment region, show partial observation frequencies of only less than 80%. In the following, the results from these under-represented areas were, therefore, not taken into account.

Averaging along the time dimension monthwise and along the local hour of the day gives a good overview to the seasonal and

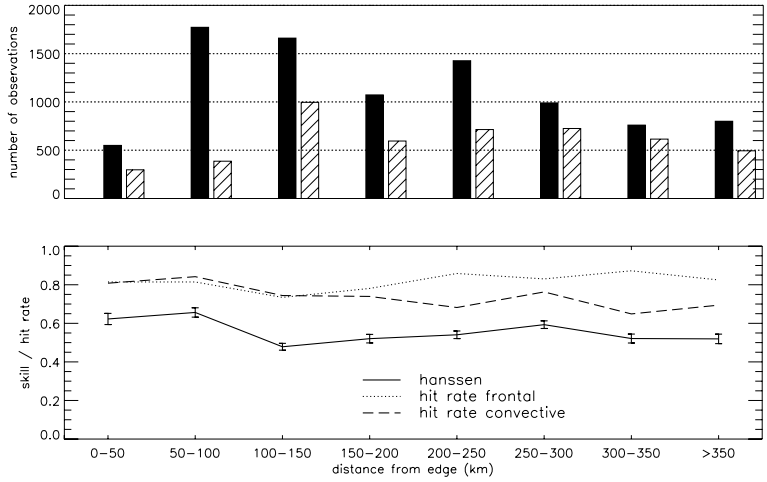

Fig. 7. Validation in dependency of the distance to the edge of the radar range. (Top): Number of SYNOP observations (filled: frontal events, streaked: convective events. (bottom): hit rates and Hanssen and Kuipers skill parameter.

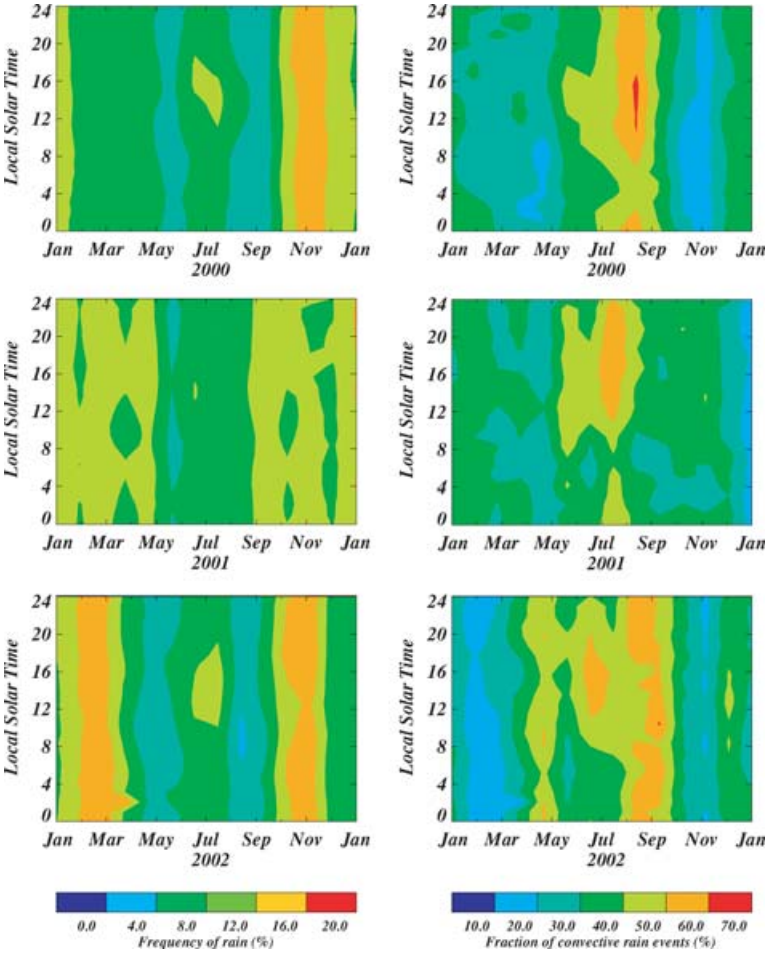

Fig. 8. Month-local solar time (LST) diagrams of frequency of rain (left) and fraction of convective rain events (right) for 2000, 2001 and 2002.

diurnal variations. The fraction of frontal events were grouped discretely by hour and month. Figure 8 illustrates the combined seasonal and diurnal cycle of precipitation frequency with intensities exceeding the threshold of 0.5 mm hr^{-1} as well as that of the convective events fraction for 2000 to 2002, respectively. On a first view of the left images, one can discern that no year is like any other with respect to the overall precipitation. In 2002 we notice two significant precipitation periods in spring and in autumn. While 2000 exhibits only one of these periods in autumn, the year 2001 features no strong precipitation period at

Table 3. Frequency of rain occurrence and fraction of frontal events

Region	area ($10^3 \cdot km^2$)	BRDC cover (%)	Fraction of wet pixel			Fraction of frontal events		
			2000	2001	2002	2000	2001	2002
Baltic Catchment	1721	76.2	10.7	11.3	11.2	0.62	0.64	0.61
Parts of Baltic Sea	415	93.3						
Baltic proper	224	94.3	9.1	10.3	11.2	0.72	0.72	0.68
Bothnian Bay	37	100	10.1	10.6	9.7	0.76	0.77	0.80
Bothnian Sea	82	100	12.6	13.5	11.5	0.80	0.82	0.81
Gulf of Finland	30	100	13.1	16.5	14.0	0.66	0.72	0.69
Gulf of Riga	16	27.5	6.8	6.9	6.0	0.73	0.69	0.70
River drainages								
Ångermanälven (Sweden)	31	100	12.5	12.1	10.2	0.73	0.64	0.57
Göta älv(Sweden)	55	100	12.4	9.7	11.6	0.76	0.72	0.75
Indalsälven(Sweden)	28	100	15.2	14.8	14.7	0.60	0.61	0.40
Kemijoki(Finland)	53	100	10.9	16.5	15.3	0.55	0.70	0.69
Neva (Russia)	261	39.1	11.1	11.8	11.4	0.62	0.67	0.65
Oder(Poland)	119	20.2	5.5	6.4	6.0	0.43	0.47	0.44
Wisla(Poland)	194	61.5	6.1	5.8	5.5	0.49	0.39	0.43
Islands								
Bornholm	0.62	100	10.8	11.3	12.8	0.53	0.46	0.49
Öland	1.3	100	9.4	11.4	12.0	0.56	0.62	0.63
Gotland	3.0	100	8.9	12.1	10.8	0.80	0.71	0.71

all. Large precipitation activity coincides with a large number of frontal overpasses with a weak diurnal cycle. The convective fraction decreases in periods with a large number of frontal overpasses to less than 20%.

During summer, rain frequencies reach levels of about 10%, with some periods exceeding 13%. The warm season is, in general, the time of convective rain and a significant diurnal cycle is noticed. Summer rainfall occurs more frequently at daytime due to an increased partition of convective rain in afternoon hours. The convective partition in summer at afternoon hours reaches peak values of more than 60%.

Table 3 summarizes the observations after separating them into the following three different parts of the Baltic area: Baltic Sea, river drainages and the large islands. We do not take into account each river catchment, but the biggest ones. The first and second column show the area and depth of coverage of the radar composites. The area size was calculated based on a catchment mask of the BALTRAD data set and are not necessarily identical to values from other geographical data sources. The values for BALTRAD cover is calculated by using the largest spatial coverage that occurred during the period. However, there are temporal gaps in the data set, mainly at the Polish radar sites. The overall maximal spatial coverage is about three-fourths of the Baltic sea catchment area. The eastern part of Baltic Sea has still a lack of radar observations, which explains why the biggest river drainage (Neva) has a BALTRAD coverage of only 39%. The yearly overall fraction of frontal events in the Baltic area is about 64% and ranges from about 40% in the more convectively influenced land surfaces to 80% in the northern Baltic Sea. The interannual variability is generally weak, especially over sea.

As mentioned above, summer is the season with the largest convective activity and, therefore, results of this seasons are very appropriate to highlight the characteristics of geographical aspect of the frontal/convective distribution. Figure 9 exhibits a map of the frontal fraction of summer season. The most prominent feature in this figure is the distinctive land-sea distribution in the northern parts of the Baltic Sea. The fraction of convective precipitation above land is significantly higher than above sea, which is assumed to be mainly caused by thermally triggered convective precipitation at daytime hours. Thus the percentage of frontal events is less than the yearly average, and the fraction of non-frontal rain increases.

6. Summary

A technique for partitioning precipitation into frontal and convective components has been presented. The method is largely independent of the absolute amount of rainfall, or radar reflectivity, thus bypassing issues associated with radar calibration. It relies on texture features and resembles classifications performed by a human observer. While this approach is inherently subjective in nature, it distinguishes different types of precipitation events and provides a tool to answer the key questions formulated in the introduction.

The method has been validated against weather reanalysis fields, as well as against synoptic data, and we find that the classification accuracy compared to both methods is roughly 80–90%.

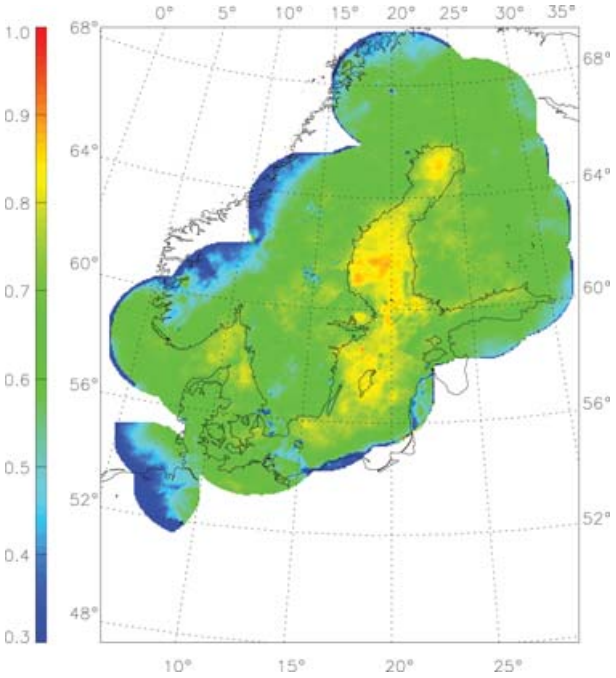

Fig. 9. Frontal fraction of overall precipitation in summer periods of 2000 to 2002. Pixels with a coverage less than 80% are masked out.

Skill scores are comparable to those found by other authors dealing with precipitation identification and/or classification, and no significant annual variability in the classification accuracy has been found.

While we use this method for the Baltic area, it is, in principle, easy to transfer to other 2-D precipitation images. The only requirements needed to apply this method are a sufficiently large areal coverage and—if one wants to apply the method without adjustments—a similar spatial resolution as that provided in the BALTRAD data set.

We have classified the type of precipitation events from 3 yr of BALTRAD radar images. The method was designed to provide estimates about the spatial distribution of precipitation, as well as seasonal and diurnal variations. It was found that frontal precipitation dominates the Baltic area, with about two-thirds of the rainfall events being frontal. The interannual variability in the investigated period was weak. However, the number of frontal events depends strongly on the season. The fraction of non-frontal events in the warm season (from May through September) is two to three times higher than in the cold season. This is caused by a higher frequency of frontal overpasses in autumn and spring and by differential heating above land surfaces in summer.

Our analyses were limited by the size of the radar composite images. All frontal systems may not be identified correctly, especially if a significant fraction of the frontal system lies outside of the radar range. Hence, it is likely that the frontal partition is even higher than in the above presented results.

The method provides the potential to investigate an important aspect of precipitation—the initial source. This information can be profitable not only in climatological studies, but also for the evaluation of weather and climate models.

7. Acknowledgments

We gratefully acknowledge Dr. Daniel Michelson (SMHI) who kindly provided the BRDC data, the gauge adjustments, and his expertise and help in processing and interpreting the data. The authors would also like to thank Prof. Jürgen Fischer for his continuous support. Rene Preusker provided the neural network program code. We are also grateful to Mark S. Kulie and Chris O'Dell for their quite constructive and informative suggestions. This work was funded by the German BMBF under contract number 01 LD 0027 in the framework of DEKLIM/BALTIMOS. Ralf Bennartz was partially funded by NASA grant NAG 5-11106.

8. Appendix A: Texture and shape parameters

GVDs are a common method to describe the texture of spatial features (Uddstrom and Gray, 1995). However, the actual definition of GVD parameters in the literature varies. Within this appendix we, therefore, briefly describe the parameters used. We employ a set of different structure measures for each precipitation area to classify its type. The parameters used here can be broadly subdivided into two classes:

(i) GVD statistics. The GVD method uses histograms of the differences between the grey values of adjacent pixels to specify texture characteristics.

(ii) Shape descriptors. This group includes the total size of a feature as well as its eccentricity as characterized by the minor and major axis of the circumscribing ellipse. These characteristics resemble the human observers capability to distinguish between long and narrow features such as rain bands and more circularly shaped rain events.

A.1 Texture information

In this study, GVDs between adjacent pixels are evaluated for each precipitation field. The corrected radar reflectivity data were transformed linearly to grey values running from 0 to 255, representing a range of reflectivities from −30 dBZ to 70 dBZ.

A GVD probability density function for a grey value image $\phi = f(x, y)$ has the form $\tilde{P}(m)$, where the m-th entry is the relative frequency of occurrence of the grey level difference $m = (|\phi(x', y') - \phi(x'', y'')| + |\phi(x', y') - \phi(x''', y''')|)/2$ for each pixel $\phi(x', y')$ and its two adjacent pixels in the eastern direction $\phi(x'', y'')$ and southern direction $\phi(x''', y''')$. At least one of these three pixels must be situated within the connected rain area. For each large contiguous precipitation field the following parameters have been calculated:

(i) **Mean grey value difference**

$$\mu = \sum_m m\widetilde{P}(m) \tag{A1}$$

which, if small, indicates that the GVD are concentrated near the origin. If the rain event is completely homogeneous the mean grey value difference would be zero. A large value corresponds to inhomogeneous precipitation fields.

(ii) **Homogeneity**

$$H = \sum_m \frac{\widetilde{P}(m)}{1+m^2} \tag{A2}$$

will be small for large GVD due to the dominance of the squared m in the denominator. Highest results will be expected if $\widetilde{P}(m)$ is high for low values of m. Thus, if the rain field is homogeneous H, will be maximal.

(iii) **Entropy**

$$E = -\sum_m \widetilde{P}(m)\log(\widetilde{P}(m)) \tag{A3}$$

indicates whether the texture is organized. This is largest when a big number of GVDs m occurs and the $\widetilde{P}(m)$ are uniformly distributed, but is small when they are highly variable.

(iv) **Contrast**

$$C = \sum_m m^2\widetilde{P}(m) \tag{A4}$$

describes the variability of the grey values in the feature. A small value of C means that small differences between adjacent pixels prevail in the image and the texture is only variable over larger distances.

These features measure various properties of the GVD probability density function, however, they are not independent from each other.

A.2 Shape descriptors

The shape parameters are based on a binary version of the precipitation fields, that is, after thresholding each pixel will be set to 'wet' or 'dry'. The parameters were defined to quantify what one can easily formulate by eye about the difference between the shape of frontal and convective precipitation systems. The most apparent features of a meteorological front are the elongated shape and an extent of at least several hundred kilometres. Thus, the chosen parameters focus on the eccentricity and the size of the area.

(i) **Size.** The size of a precipitation field, A, is simply the number of pixels n_{rain} with rain in the contiguous area.

(ii) **Length of the major axis.** The length of the first principal component axis refers to the largest dimension of the shape.

(iii) **Eccentricity.** The ratio of the longest chord perpendicular to the first principal axis to the first principal axis itself. The eccentricity factor may take values from almost zero (high eccentricity, long narrow features) to one (both major axes have the same length, e.g. circular shape). High eccentricity is typically associated with frontal rain areas.

(iv) **Compactness.** The entire area used for this parameter includes each wet pixel identified as a part of the connected rain field, and additionally each pixel which is less than 20 km to the perimeter of this particular rain field. For our study we defined compactness as the ratio of the number of rain pixels to the number of all pixels within the area circumscribing the precipitation field.

References

Anagnostou, N. E. and Kummerow, C. 1997. Stratiform and convective classification of rainfall using SSM/I 85-Ghz brightness temperature observations. *J. Atmos. Oceanic Technol.* **14**, 570–575.

Appleman, H. S. 1960. A fallacy in the use of skill scores. *Bull. Amer. Meteor.* **41**, 64–67.

Biggerstaff, M. and Listemaa, S. 2000. An improved scheme for convective/stratiform echo classification using radar reflectivity. *Journal of Applied Meteorology* **39**, 2129–2150.

Brier, G. W. and Allen, R. A. 1952. Verification of weather forecasts. In: *Compendium of Meteorology, Amer. Meteor. Soc. Boston,* 841–848.

Hanssen, A. W. and Kuipers, W. 1965. On the relationship between the frequency of rain and various meteorological parameters. Koninklijk Nederlands Meteorologisch Institut. *Meded. Verhand.* **81**, 2–15.

Heidke, P. 1926. Berechnung des Erfolges und der Güte der Windstärkevorhersagen im Sturmwarnungsdienst. *Geogr. Ann.* **8**, 301–349.

Marquard, A. 1963. An algorithm for least-squares estimation of nonliniear parameters. *SIAM J. Appl. Math.* **11**, 413–441.

Michelson, D., Andersson, T., Koistinen, J., Collier, C., Riedl, J. and co-authors, 2000. BALTEX Radar DATA Centre Products and their Methodologies. Technical Report RMK 90, SMHI, SE-60176 Norrköping, Sweden.

Pankiewicz, G. S. 1997. Neural network classification of convective air masses for a flood forecating system. *Int. J. Remote Sensing* **18**, 887–898.

Rumelhart, D. and McClelland, J. 1986. *Parallel Distributed Processing Vol. 1.* Cambridge, MA, MIT press, 547 pp.

Schowengerdt, R., 1997. *Remote sensing, models and methods for image processing.* Academic press, 522 pp.

Shepherd, G. W., Cluckie, I. D., Collier, C. G., Yu, S. and James, P. K. 1988. The identification of rainfall type from weather radar data. *Meteorological Magazine* **117**, 180–186.

Skomorowski, P., Clemens, M., Bumke, K., Rudolf, B. and Rubel, F. 2003. Observed precipitation climatology for the Baltic. *Geophysical Research Abstracts* **5**, 10 133.

Steiner, M., Houze, R. A. Jr. and Yuter, S. 1995. Climatological characterizations of three-dimensional storm structure from operational radar and rain gauge data. *Journal of Applied Meteorology* **34**, 1978–2007.

Sumner, G. N. 1988. *Precipitation: Process and Analysis.* John Wiley & Sons Ltd., New York, 455 pp.

Tetzlaff, G. and Hagemann, N. 1986. Bemerkungen zum Niederschlag in Hannover. *Meteorologische Rundschau* **39**, 1–12.

Tian, B., Shaikh, M. A., Azimi-Sadjadi, M. R., Vonder Haar, T. H. and Reinke, D. L. 1999. A study of cloud classification with neural networks using spectral and textural features. *IEEE Transactions on Neural Networks* **10**(1), 138–151.

Uddstrom, M. J. and Gray, W. 1995. Satellite cloud classification and rain-rate estimation using multispectral radiances and measures of spatial texture. *Journal of Applied Meteorology* **35**, 839–858.

Woodcok, F. 1976. The Evaluation of Yes/No Forecasts for Scientific and Administrative Purposes. *Monthly Weather Review* **104**, 1209–1214.